

Hardy space infinite elements for Helmholtz-type problems with unbounded inhomogeneities [☆]

Lothar Nannen^a, Achim Schädle^b

^a*Institut für Numerische und Angewandte Mathematik, Georg-August Universität
Göttingen, Lotzestraße 16-18, 37083 Göttingen, Germany*

^b*Mathematisches Institut, Heinrich-Heine Universität Düsseldorf, Universitätsstraße 1,
40225 Düsseldorf, Germany*

Abstract

This paper introduces a class of approximate transparent boundary conditions for the solution of Helmholtz-type resonance and scattering problems on unbounded domains. The computational domain is assumed to be a polygon. A detailed description of two variants of the Hardy space infinite element method which relies on the pole condition is given. The method can treat waveguide-type inhomogeneities in the domain with non-compact support. The results of the Hardy space infinite element method are compared to a perfectly matched layer method. Numerical experiments indicate that the approximation error of the Hardy space decays exponentially in the number of Hardy space modes.

Keywords: Helmholtz, resonance, scattering, transparent boundary condition, non-reflecting boundary condition, pole condition, Hardy space, infinite element method

1. Introduction

To solve numerically the Helmholtz equation

$$-\Delta u(x) - \kappa^2 n(x)u(x) = 0, \quad x \in \Omega \quad (1)$$

on an unbounded domain Ω with some boundary conditions on $\partial\Omega$ and a radiation condition at infinity, the computational domain is typically restricted to a bounded interior Ω_{int} . Here $n(x)$ is the refraction index and κ is the wavenumber. In case of a scattering problem $\kappa > 0$ is given, whereas in case of a resonance problem κ with positive real part is the sought resonance. Applying transparent boundary conditions at the artificial interface Γ of the exterior/interior domain, the problem can be restricted to solving the Helmholtz equation on the interior domain only. Transparent boundary conditions on Γ have to model the correct radiation condition at infinity.

[☆]This work was supported by the Deutsche Forschungsgemeinschaft (DFG).

For homogeneous exterior domains and $\kappa > 0$ the correct radiation condition is the Sommerfeld radiation condition. It is known that the exact transparent boundary condition, i.e. the Calderon or Dirichlet-to-Neumann map, is non-local. Currently used methods to approximate or realize transparent boundary conditions are based on separable coordinates and special functions [7], infinite elements [1, 4], perfectly matched layer (PML) constructions [26, 2, 3], boundary integral approaches [14] and local high order approximations [6].

Except for some PML methods they depend non-linearly on κ^2 , which is a severe drawback when solving resonance problems, where one seeks non-trivial eigenpairs (u, κ^2) for (1) with vanishing boundary conditions on $\partial\Omega$ and a radiation condition at infinity. Using finite elements to discretize (1) in $H^1(\Omega_{\text{int}})$ leads to a generalized eigenvalue problem. Employing transparent boundary conditions, that are non-linear in the eigenvalue, would make the eigenvalue problem non-linear. Although it is possible to solve the resulting non-linear eigenvalue problems, see e.g. [19], it is reasonable to avoid them. Therefore PML methods are currently the standard method for solving resonance problems, see e.g. [9, 17]. Under the name *complex scaling* they have been used since the 1970s for the theoretical study and the numerical computation of resonances in molecular physics [26]. Unfortunately these methods give rise to spurious resonance modes and several parameters have to be optimized for each problem. The PML method we use to check the results of our Hardy space infinite element method choses the thickness and the discretization of the layer adaptively [27, 22].

The theoretical framework of the Hardy space infinite element (HSIE) method is the pole condition by F. Schmidt [23, 24]. The pole condition considers the Laplacetransform of the exterior solution with respect to some generalized distance variable. A solution is then called (purely) outgoing if this Laplacetransform has no singularity in the lower complex half plane, vice versa a solution is (purely) incoming if its Laplacetransform has no singularity in the upper complex half plane. In [13] it is shown that for homogeneous exterior domains this condition on the singularities of the Laplacetransform, i.e. all its singularities are located in the upper complex half, is equivalent to the Sommerfeld radiation condition.

Compared to former numerical realizations of the real axis approach of the pole condition [12], which were based on BDF and Runge-Kutta methods, the HSIE method which is based on a Galerkin method in the Hardy space $H^+(D)$ of the complex unit disk, shows exponential convergence and is simple to implement in finite element codes. It was first presented in [20, 11] for homogeneous exterior domains with spherical interface Γ . The cut function approach of the pole condition [12] was discretized in [25] using a collocation method in some sort of Hardy space and shows exponential convergence in experiments, too. Moreover it allows for the evaluation of the exterior field. However this approach is not linear in κ^2 and exhibits problems concerning the stability under perturbations of the boundary data.

Extending [11] we assume here that the interface Γ is the boundary of a convex polygon P , i.e. $\Omega_{\text{int}} = P \cap \Omega$ and $\Omega_{\text{ext}} = \mathbb{R}^2 \setminus P$, and that the exte-

rior domain Ω_{ext} is discretized by infinite trapezoids, such that the refractive index $n(x)$ of (1) is constant on each trapezoid. These trapezoids are the images of bilinear mappings from a reference strip. The infinite direction of this reference strip is mapped into the Hardy space $H^+(D)$, where a L^2 -orthogonal basis is given by trigonometric monomials. The basis functions of our Galerkin method are therefore tensor products of standard finite element functions with the trigonometric monomials in the Hardy space.

The method presented here treats scattering problems as well as the corresponding resonance problems. The pole condition as a mean to realize transparent boundary conditions for time dependent problems is considered in [21]. The discretization used there is almost equivalent to one employed here.

In section 2 we present the HSIE method from a practical point of view first in one dimension and then in two dimensions. In section 3 we shortly review the PML method used here. Numerical results are presented in section 4 with a comparison of both methods.

2. Hardy space infinite element method

To explain the basic ideas of HSIEs we shortly discuss one-dimensional problems, even though for such problems there exist simpler and more efficient methods to treat the unboundedness of the domain. Nevertheless, as the multi-dimensional elements are tensor products of standard finite elements and one-dimensional infinite elements, it is useful to start with the simple case.

2.1. One-dimensional elements

We consider the Helmholtz equation

$$-u''(r) - \kappa^2 n(r)u(r) = 0, \quad r \geq 0, \quad (2a)$$

$$u'(0) = g, \quad (2b)$$

$$u \quad \text{is outgoing} \quad (2c)$$

with complex wave number $\kappa \in \mathbb{C}$ with positive real part ($\Re(\kappa) > 0$), boundary value $g \in \mathbb{C}$, and positive potential $n \in L^\infty((0, \infty))$ satisfying $n(r) = 1$ for $r \geq a$ for some a . The Sommerfeld radiation condition

$$\lim_{r \rightarrow \infty} (\partial_r u(r) - i\kappa u(r)) = 0$$

guarantees for κ with nonnegative imaginary part ($\Im(\kappa) \geq 0$) that (2) is well-posed and that the solution u is outward radiating. Solutions to (2a) may be decomposed into an interior part $u_{\text{int}} := u|_{[0,a]}$ and an exterior part $u_{\text{ext}}(r) := u(r+a)$, $r \geq 0$, with

$$u_{\text{ext}}(r) = C_1 e^{i\kappa r} + C_2 e^{-i\kappa r} \quad \text{and} \quad C_1 + C_2 = u_{\text{int}}(a).$$

The term $C_1 e^{i\kappa r}$ corresponds to an outgoing radiating wave, that satisfies the Sommerfeld radiation condition, and $C_2 e^{-i\kappa r}$ corresponds to an incoming wave.

Therefore $C_2 = 0$ and hence $u_{\text{ext}}(r) = u_{\text{int}}(a)e^{i\kappa r}$. The solution of (2) restricted to $[0, a]$ is thus given by the simple boundary value problem

$$-u_{\text{int}}''(r) - n(r)\kappa^2 u_{\text{int}}(r) = 0, \quad u_{\text{int}}'(0) = g, \quad u_{\text{int}}'(a) = i\kappa u_{\text{int}}(a). \quad (3)$$

Thus in the one-dimensional case the Sommerfeld radiation condition is satisfied at the boundary of the interior domain. Therefore it can be used for κ with negative imaginary part, too.

Note that the resonance problem corresponding to (3) leads to a quadratic eigenvalue problem in κ whereas the discretization using Hardy space infinite elements will lead to an eigenvalue problem that is linear in κ^2 .

Hardy space infinite elements rest on the fact, that the Laplace transform of the exterior solution

$$(\mathcal{L}u_{\text{ext}})(s) := \int_0^\infty e^{-sr} u_{\text{ext}}(r) dr, \quad \Re(s) \geq |\Im(\kappa)|$$

has a holomorphic extension except for two poles at $\pm i\kappa$

$$\mathcal{L}\{C_1 e^{i\kappa \bullet} + C_2 e^{-i\kappa \bullet}\}(s) = \frac{C_1}{s - i\kappa} + \frac{C_2}{s + i\kappa}.$$

Hence, u_{ext} is outgoing if and only if $\mathcal{L}u_{\text{ext}}$ has no poles with negative imaginary part. An equivalent formulation in terms of an appropriate Hardy space is given in Definition 2.

Definition 1 (Hardy space). Let $P_{\kappa_0}^- = \{s \in \mathbb{C} : \Im(s/\kappa_0) < 0\}$ be the half plane below the line $\kappa_0\mathbb{R}$ through the origin and κ_0 , see Fig. 2.1. The *Hardy space* $H^-(P_{\kappa_0}^-)$ is the space of all functions f , that are holomorphic in $P_{\kappa_0}^-$, such that

$$\int_{\mathbb{R}} |f(\kappa_0 x - \kappa_0 i\epsilon)|^2 dx$$

is uniformly bounded for $\epsilon > 0$.

Let $D = \{s \in \mathbb{C} : |s| < 1\}$ be the open unit disk. The *Hardy space* $H^+(D)$ is the space of all functions f , that are holomorphic in D , such that

$$\int_0^{2\pi} |f(re^{it})|^2 dt$$

is bounded uniformly for $r \in [0, 1)$.

Due to the uniform boundedness of f there exist in both cases a L^2 function on the boundary, which is uniquely determined by f and which determines vice versa uniquely the function in the domain. Hence, we identify a Hardy space function $f \in H^-(P_{\kappa_0}^-)$ or $f \in H^+(D)$ with its boundary function $f \in L^2(\kappa_0\mathbb{R})$ and $f \in L^2(S^1)$ respectively.

Definition 2 (Pole condition). Let κ_0 be a complex constant with positive real part and $\Re(\kappa/\kappa_0) > 0$. Then a solution u to (2a) is said to obey the pole condition and is called outgoing, if the holomorphic extension of the Laplace transform of the exterior part lies in the Hardy space $H^-(P_{\kappa_0}^-)$.

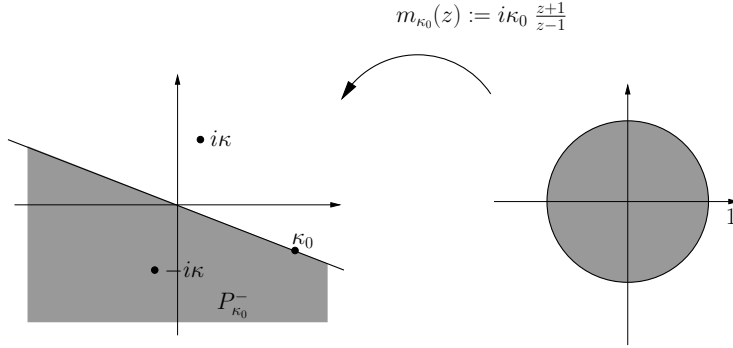


Figure 1: sketch to definition 1

The constant κ_0 will act as a tuning parameter in the method presented below. In future we omit the formulation "holomorphic extension of the Laplace transform" and shortly write Laplace transform \mathcal{L} . The Hardy space $H^-(P_{\kappa_0}^-)$ is a Hilbert space [5, 10], with the standard L^2 -norm, and the following Lemma connects the two Hardy spaces $H^-(P_{\kappa_0}^-)$ and $H^+(D)$.

Lemma 3 (Möbius transform). *The mapping*

$$\mathcal{M}_{\kappa_0} : H^-(P_{\kappa_0}^-) \rightarrow H^+(D) : f \mapsto (\mathcal{M}_{\kappa_0} f)(z) := f\left(i\kappa_0 \frac{z+1}{z-1}\right) \frac{1}{z-1} \quad (4)$$

is up to a factor $\sqrt{2|\kappa_0|}$ unitary.

Due to the explicit knowledge of u_{ext} the transformed function $\hat{U} := \mathcal{M}_{\kappa_0} \mathcal{L} u_{\text{ext}}$ is given by

$$\hat{U}(z) = \frac{u_{\text{int}}(a)}{i\kappa_0(z+1) - i\kappa(z-1)} = \frac{u_{\text{int}}(a)}{i(\kappa + \kappa_0)} \sum_{j=0}^{\infty} \left(\frac{\kappa - \kappa_0}{\kappa + \kappa_0}\right)^j z^j. \quad (5)$$

Since $\left|\frac{\kappa - \kappa_0}{\kappa + \kappa_0}\right| < 1$, we could expect exponential convergence for the exterior solution, if we use the first $N + 1$ trigonometric monomials $\{z^0, z^1, \dots, z^N\}$ as a Galerkin basis of the space $H^+(D)$. For the interior part $u_{\text{int}} \in H^1([0, a])$ we use a standard finite element method.

Both methods have the term $u_{\text{int}}(a)$ in common and we call the associated boundary degree of freedom u_0 . As usual it couples the finite elements for the interior part with the infinite elements for the exterior part. Note, that in the formulation (5) all degrees of freedom for \hat{U} would couple with $u_{\text{int}}(a)$, since $u_{\text{int}}(a) = 2i\kappa_0 \hat{U}(1)$. In order to get a local coupling of the boundary degree of freedom and the inner degrees of freedom, we decompose $\hat{U} = \frac{1}{i\kappa_0} \mathcal{T}_-(u_0, U)^\top$ with

$$\mathcal{T}_- \begin{pmatrix} u_0 \\ U \end{pmatrix} (z) := \frac{1}{2} (u_0 + (z-1)U(z)) \quad (6)$$

for $(u_0, U)^\top \in \mathbb{C} \times H^+(D)$ and use the trigonometric monomials as a basis for U .

It remains to derive a variational formulation for $(u_{\text{int}}, U)^\top$ in $H^1([0, a]) \times H^+(D)$, which was done in [11]. Here $H^1([0, a])$ is the Sobolev space of weakly differentiable functions on the interval $[0, a]$. The basic idea is to use the properties of the Fourier transform to get the identity

$$\int_0^\infty f(r)g(r)dr = -2i\kappa_0 A(\mathcal{M}_{\kappa_0} \mathcal{L}f, \mathcal{M}_{\kappa_0} \mathcal{L}g) \quad (7)$$

with

$$A(F, G) := \frac{1}{2\pi} \int_{S^1} F(\bar{z})G(z)|dz|, \quad F, G \in H^+(D). \quad (8)$$

This holds for u_{ext} and suitable test functions v_{ext} , as well as for the derivatives u'_{ext} and v'_{ext} . Using the decomposition $\mathcal{M}_{\kappa_0} \mathcal{L}u_{\text{ext}} = \frac{1}{i\kappa_0} \mathcal{T}_-(u_0, U)^\top$ and $\mathcal{M}_{\kappa_0} \mathcal{L}v_{\text{ext}} = \frac{1}{i\kappa_0} \mathcal{T}_-(v_0, V)^\top$ we obtain simple formulas for the derivatives of u_{ext} and v_{ext}

$$\mathcal{M}_{\kappa_0} \mathcal{L}f' = \mathcal{T}_+ \begin{pmatrix} f_0 \\ F \end{pmatrix} \quad \text{with } \mathcal{T}_+ \begin{pmatrix} f_0 \\ F \end{pmatrix} (z) := \frac{1}{2} (f_0 + (z+1)F(z)). \quad (9)$$

Now we are able to deduce from the formal variational formulation of (2a)

$$\int_0^a (u'_{\text{int}} v'_{\text{int}} - \kappa^2 n u_{\text{int}} v_{\text{int}}) dr + \int_0^\infty (u'_{\text{ext}} v'_{\text{ext}} - \kappa^2 n u_{\text{ext}} v_{\text{ext}}) dr = -g v_{\text{int}}(0)$$

and (7) the variational equation in $H^1([0, a]) \times H^+(D)$:

$$B \left(\begin{pmatrix} u_{\text{int}} \\ U \end{pmatrix}, \begin{pmatrix} v_{\text{int}} \\ V \end{pmatrix} \right) = -g v_{\text{int}}(0) \quad (10)$$

with

$$\begin{aligned} B \left(\begin{pmatrix} u_{\text{int}} \\ U \end{pmatrix}, \begin{pmatrix} v_{\text{int}} \\ V \end{pmatrix} \right) &:= \int_0^a (u'_{\text{int}} v'_{\text{int}} - \kappa^2 n u_{\text{int}} v_{\text{int}}) dr \\ &- 2i\kappa_0 A \left(\mathcal{T}_+ \begin{pmatrix} u_0 \\ U \end{pmatrix}, \mathcal{T}_+ \begin{pmatrix} v_0 \\ V \end{pmatrix} \right) - \frac{2i\kappa^2}{\kappa_0} A \left(\mathcal{T}_- \begin{pmatrix} u_0 \\ U \end{pmatrix}, \mathcal{T}_- \begin{pmatrix} v_0 \\ V \end{pmatrix} \right). \end{aligned}$$

Since for the trigonometric monomials $A(z^j, z^k) = \delta_{j,k}$, the implementation of the exterior part of the bilinear form B reduces to the implementation of the operators $\mathcal{T}_\pm : \mathbb{C} \times H^+(D) \rightarrow H^+(D)$, if the finite dimensional ansatz space $\Pi_N := \text{span}\{z^0, z^1, \dots, z^N\}$ is used for $H^+(D)$:

$$\mathcal{T}_{N,\pm} := \frac{1}{2} \begin{pmatrix} 1 & \pm 1 & & & \\ & \ddots & \ddots & & \\ & & & 1 & \pm 1 \\ & & & & 1 \end{pmatrix}. \quad (11)$$

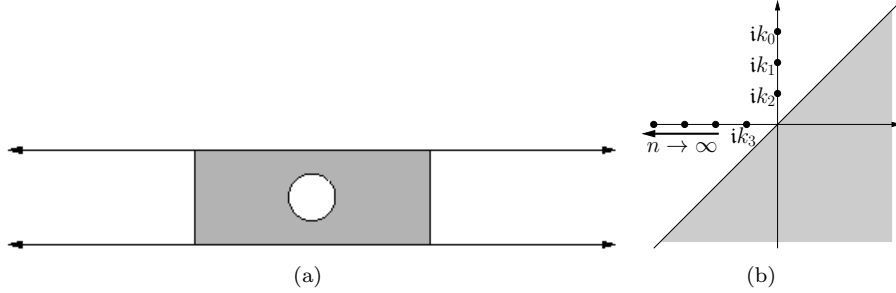


Figure 2: a) 2d waveguide with bounded inhomogeneity, b) poles of the Laplace transform of the different waveguide modes

The first row in these matrices correspond to the boundary degree of freedom u_0 . The local element matrix for the infinite element is then given by

$$-2i\kappa_0 \mathcal{T}_{N,+}^\top \mathcal{T}_{N,+} - \kappa^2 \frac{2i}{\kappa_0} \mathcal{T}_{N,-}^\top \mathcal{T}_{N,-}.$$

Note that it is linear in κ^2 and the matrices are explicitly known. In [11] the equivalence of the variational equation in $H^1([0, a]) \times H^+(D)$ and the classical problem (2) is shown. Moreover, the stability of the Hardy space infinite element method follows with a Gårding inequality and exponential convergence in the number of degrees of freedom N for the Hardy space is proven.

Remark 4. In the space domain the monomial basis functions z^j correspond to the functions

$$u_j(r) = e^{i\kappa_0 r} \left\{ u_0 + \sum_{n=0}^j \binom{j}{n} \frac{(2i\kappa_0 r)^{n+1}}{(n+1)!} \right\}.$$

Therefore for the one dimensional problem an optimal choice for scattering problems is $\kappa_0 = \kappa$ since in this case the exact transparent boundary condition is obtained even with no degrees of freedom in $H^+(D)$. For resonance problems, κ_0 should be chosen in the region of the complex plane where resonances are of interest.

2.2. Tensor product elements for a semi-infinite strip

For the multi-dimensional case we first present the extension of the one-dimensional Hardy space method to Helmholtz problems for waveguides with locally bounded inhomogeneities like the circle in Fig. 2(a). Given some incoming wave u_i satisfying the homogeneous Helmholtz equation $-\Delta u_i - \kappa^2 u_i = 0$, the total wave u is the sum of u_i and a scattered wave u_s , which has to satisfy

a radiating condition. The problem is given by

$$-\Delta u(x, y) - \kappa^2 u(x, y) = 0, \quad (x, y) \in \Omega \subset \mathbb{R} \times [0, \pi], \quad (12a)$$

$$\partial_\nu u = 0 \quad \text{on } \partial\Omega, \quad (12b)$$

$$\mathcal{M}_{\kappa_0} \mathcal{L} u_s(\bullet, y) \in H^+(D), \quad y \in [0, \pi]. \quad (12c)$$

The Laplace transform in (12c) is applied for fixed tangential variable y to the scattered wave u_s outside the gray shaded domain, i.e. for x in both directions $\pm\infty$. Note, that u_s can be written as a superposition of one-dimensional waves with wavenumbers $k_n := \sqrt{\kappa^2 - n^2}$

$$u_s(x, y) = \sum_{n=0}^{\infty} c_n \cos(ny) e^{ik_n x}. \quad (13)$$

As sketched in Fig. 2(b) there exist only a few guided modes and infinitely many evanescent modes. The parameter κ_0 in the Möbius transform has to be adapted to the region, where the Laplace transforms for all these modes are holomorphic. This way the results of [13, 11] carry over to the waveguide problem (12), even though this is not directly contained in these papers.

In the gray shaded domain $\Omega_{\text{int}} := \Omega \cap [a, b] \times [0, \pi]$ of Fig. 2(a) we use a standard finite element method to approximate the total wave u . Since only the scattered wave satisfies the radiation condition, we have to solve the problem in the exterior domains for u_s and not for u . On the artificial boundary Γ , that separates Ω_{int} from Ω_{ext} this gives rise to a jump condition for the Dirichlet values as well as an additional boundary term from the jump in the Neumann values:

$$\begin{aligned} & \int_{\Omega_{\text{int}}} (\nabla u \cdot \nabla v - \kappa^2 uv) dx dy + \int_0^\pi \int_{-\infty}^a (\nabla u_s \cdot \nabla v - \kappa^2 u_s v) dx dy \\ & + \int_0^\pi \int_b^\infty (\nabla u_s \cdot \nabla v - \kappa^2 u_s v) dx dy = \int_0^\pi ((\partial_x u_i)(b, y)v(b, y) - (\partial_x u_i)(a, y)v(a, y)) dy \end{aligned}$$

for suitable test functions v . The infinite integrals can be transformed into the Hardy space using (7) and as in the one-dimensional case the decomposition (6), which ensures the continuity of the solution over the interfaces. E. g. for $x \geq b$ the stiffness and mass integral become

$$\begin{aligned} \int_0^\pi \int_b^\infty \nabla u_s \cdot \nabla v dx dy &= -2i\kappa_0 \int_b^\infty A\left(\mathcal{T}_+\left(\begin{array}{c} u_{s0}(y) \\ U(\bullet, y) \end{array}\right), \mathcal{T}_+\left(\begin{array}{c} v_0(y) \\ V(\bullet, y) \end{array}\right)\right) dy \\ &+ \frac{2i}{\kappa_0} \int_b^\infty A\left(\partial_y \mathcal{T}_-\left(\begin{array}{c} u_{s0}(y) \\ U(\bullet, y) \end{array}\right), \partial_y \mathcal{T}_-\left(\begin{array}{c} v_0(y) \\ V(\bullet, y) \end{array}\right)\right) dy, \quad (14a) \end{aligned}$$

$$\int_0^\pi \int_b^\infty u_s v dx dy = \frac{2i}{\kappa_0} \int_b^\infty A\left(\mathcal{T}_-\left(\begin{array}{c} u_{s0}(y) \\ U(\bullet, y) \end{array}\right), \mathcal{T}_-\left(\begin{array}{c} v_0(y) \\ V(\bullet, y) \end{array}\right)\right) dy \quad (14b)$$

Since on the interface $[0, \pi]$ there already exists a discretization consisting of the traces $b_m^{(y)}$ of finite element basis functions in the interior domain, we use these

basis functions for the boundary values u_{s_0} and v_0 :

$$u_{s_0}(y) = \sum_{m=0}^{N_m} c_m b_m^{(y)}(y), \quad y \in [0, \pi].$$

For $U, V \in H^+(D) \otimes H^{1/2}([0, \pi])$ it is reasonable to use tensor product elements:

$$U(z, y) = \sum_{m=0}^{N_m} \sum_{i=0}^{N_i} c_{m,i} z^i b_m^{(y)}(y), \quad z \in S^1, \quad y \in [0, \pi].$$

In this way the integrals (14) give rise to tensor products of the boundary matrices

$$S_{mn}^{\text{bd}} = \int_0^\pi \partial_y b_m^{(y)}(y) \partial_y b_n^{(y)}(y) dy, \quad M_{mn}^{\text{bd}} = \int_0^\pi b_m^{(y)}(y) b_n^{(y)}(y) dy \quad (15)$$

and the Hardy space matrices $S^{\text{HSM}} = -2i\kappa_0 \mathcal{T}_{N,+}^\top \mathcal{T}_{N,+}$ and $M^{\text{HSM}} = \frac{2i}{\kappa_0} \mathcal{T}_{N,-}^\top \mathcal{T}_{N,-}$:

$$S_{\text{ext}} = S^{\text{HSM}} \otimes M^{\text{bd}} + M^{\text{HSM}} \otimes S^{\text{bd}}, \quad M_{\text{ext}} = M^{\text{HSM}} \otimes M^{\text{bd}}. \quad (16)$$

2.3. Tensor product elements

In the general multi-dimensional case we consider the Helmholtz equation

$$-\Delta u(x, y) - \kappa^2 n(x, y) u(x, y) = 0, \quad (x, y) \in \Omega, \quad (17)$$

with a potential n , an unbounded domain Ω , with some boundary condition on $\partial\Omega$ and as a radiation condition the pole condition along a generalized radial direction for u . Soon it will become clear what is meant by a generalized radial direction of u . The assumptions on the potential n will be given in Remark 7.

In [11] the computational domain is obtained by intersecting Ω with a ball B_a of radius a , $\Omega_{\text{int}} := B_a \cap \Omega$, such that the unbounded exterior is $\Omega_{\text{ext}} := \mathbb{R}^d \setminus B_a$. Using polar coordinates in Ω_{ext} and separation of variables the unbounded radial direction and the bounded surface directions separate. Hence, the one-dimensional approach can be applied to the radial part of the exterior solution and a standard finite element method handles the interior part as well as the bounded surface directions.

However the boundary of Ω_{ext} need not be a sphere, arbitrary convex polygons P can be used to split Ω into $\Omega_{\text{ext}} := \Omega \setminus P$ and $\Omega_{\text{int}} := P \cap \Omega$ with interface $\Gamma := \partial P$. Here for simplicity we present only the two-dimensional case. In Fig. 2.3 two different segmentations of the exterior domain are illustrated: The left one decomposes the exterior into semi-infinite strips and infinite triangles, while the right one uses semi-infinite trapezoids.

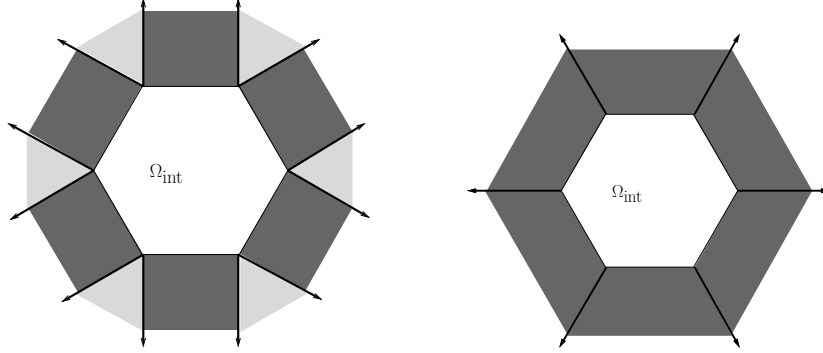


Figure 3: different segmentations of the exterior domain

2.3.1. Infinite triangles and strips

We first present the Hardy space infinite element method for the segmentation using infinite triangles and strips. For the semi-infinite strips we use the elements from section 2.2. Hence only the implementation of the method for the infinite triangles is considered below. If P is the vertex of such an infinite triangle and n_1 and n_2 are the unit normal vectors of the neighboring strips, then the triangle is given by $T = \mathbf{g}([0, \infty) \times [0, \infty))$ with the linear mapping

$$\mathbf{g}(\xi, \eta) = P + \xi n_1 + \eta n_2, \quad (\xi, \eta) \in [0, \infty) \times [0, \infty). \quad (18)$$

If we define $\hat{u}(\xi, \eta) := u(\mathbf{g}(\xi, \eta))$ on the reference, then with the constant Jacobi matrix J of \mathbf{g} , the mass and stiffness integrals for the infinite triangle are transformed according to

$$\begin{aligned} \int_T u v d(x, y) &= \int_{[0, \infty) \times [0, \infty)} \hat{u} \hat{v} |J| d(\xi, \eta), \\ \int_T \nabla_{xy} u \cdot \nabla_{xy} v d(x, y) &= \int_{[0, \infty) \times [0, \infty)} J^{-T} \nabla_{\xi\eta} \hat{u} \cdot J^{-T} \nabla_{\xi\eta} \hat{v} |J| d(\xi, \eta). \end{aligned} \quad (19)$$

In contrast to the strips, the integrals include the Jacobi matrix and there are two infinite directions to which (7) is applied to. If we define the constant matrix $G := |J|J^{-1}J^{-T}$, then the local element matrices for each infinite triangle T are given by

$$\begin{aligned} S_T &= G_{11} S^{\text{HSM}} \otimes S^{\text{HSM}} + G_{12} S^{\text{HSM}} \otimes M^{\text{HSM}} \\ &\quad + G_{21} M^{\text{HSM}} \otimes S^{\text{HSM}} + G_{22} M^{\text{HSM}} \otimes M^{\text{HSM}}, \\ M_T &= |J| M^{\text{HSM}} \otimes M^{\text{HSM}}. \end{aligned} \quad (20)$$

Remark 5. In the transformation \mathbf{g} we use the unit normal vectors, which guarantees the continuity of the solution along the infinite rays.

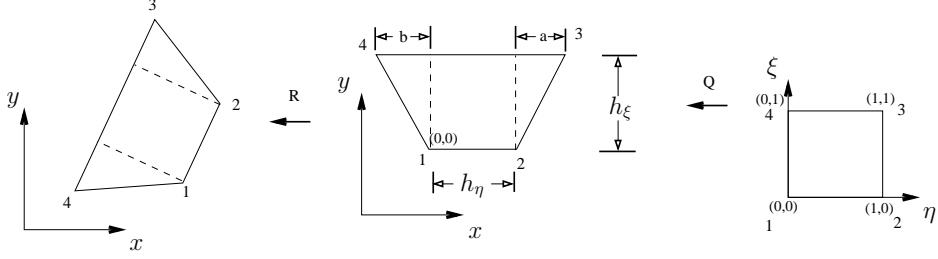


Figure 4: Transformation of each trapezoid

2.3.2. Infinite trapezoids

The method presented in 2.3.1 has the advantage to be easy to implement, but it results in extra degrees of freedom in the infinite triangles. The second method avoids these degrees of freedom by using infinite trapezoids. The infinite rays, which are no longer normal to the boundary, could e.g. be constructed in 2d with bisecting lines. Another possibility is to choose a reference point P_0 in the interior domain and construct the rays R for each vertex V of the boundary by $R = V - P_0$. General conditions for suitable segmentations in infinite trapezoids may be found in [24, 28, 16].

Given a segmentation with finite trapezoids, the trapezoid element is the image of a reference rectangle (see Fig. 4) under the affine bilinear mapping \mathbf{g} with

$$(x, y) = \mathbf{g}(\eta, \xi) = R \circ Q(\eta, \xi) + (x_1, y_1)^T, \quad (21)$$

where

$$(x, y) = Q(\eta, \xi) = \begin{pmatrix} h_\eta \eta - b\xi + (a+b)\eta\xi \\ h_\xi \xi \end{pmatrix} \quad (22)$$

with $h_\eta = \sqrt{(x_2 - x_1)^2 + (y_2 - y_1)^2}$, $a = (x_4 - x_3, y_4 - y_3)(x_2 - x_3, y_2 - y_3)^T / \|(x_4 - x_3, y_4 - y_3)\|_2$, $b = (x_3 - x_4, y_3 - y_4)(x_1 - x_4, y_1 - y_4)^T / \|(x_3 - x_4, y_3 - y_4)\|_2$ and $h_\xi = \sqrt{\|(x_3 - x_2, y_3 - y_2)\|_2^2 - a^2}$. Note, that a and b are signed distance variables.

Remark 6. The variable ξ plays the role of a generalized radial variable, whereas η is the surface variable on Γ . To guarantee continuity of the discrete solution in the exterior domain it is important, that the radial variable ξ along the rays of the segmentation is independent of the neighboring infinite elements. This is fulfilled, if two neighboring (finite) trapezoids have the same boundary vertices.

The rotation R is given by

$$(\hat{x}, \hat{y}) = R(\tilde{x}, \tilde{y}) = \frac{1}{\sqrt{(x_2 - x_1)^2 + (y_2 - y_1)^2}} \begin{pmatrix} x_2 - x_1 & y_1 - y_2 \\ y_2 - y_1 & x_2 - x_1 \end{pmatrix}. \quad (23)$$

The Jacobi matrix J of the transformation \mathbf{g} and its determinant are

$$J = \begin{pmatrix} h_\eta + (a+b)\xi & -b + (a+b)\eta \\ 0 & h_\xi \end{pmatrix}, \quad |J| = h_\xi(h_\eta + (a+b)\xi) \quad (24)$$

and the inverse of J is

$$J^{-1} = \begin{pmatrix} \frac{1}{h_\eta + \xi(a+b)} & \frac{b - (a+b)\eta}{h_\xi(h_\eta + \xi(a+b))} \\ 0 & \frac{1}{h_\xi} \end{pmatrix}. \quad (25)$$

Note, that J is no longer constant. Mass and stiffness integral transform as in (19)

$$\begin{aligned} \int_T u v d(x, y) &= \int_{[0,1] \times [0,\infty]} \hat{u} \hat{v} |J| d(\eta, \xi), \\ \int_T \nabla_{xy} u \cdot \nabla_{xy} v d(x, y) &= \int_{[0,1] \times [0,\infty]} J^{-T} \nabla_{\eta\xi} \hat{u} \cdot J^{-T} \nabla_{\eta\xi} \hat{v} |J| d(\eta, \xi). \end{aligned} \quad (26)$$

As before we use tensor product basis functions on the reference element $\hat{b}_{m,i} := \hat{b}_m^{(\eta)} \otimes \hat{b}_i^{(\xi)}$. Again the integrals decouple, such that for the mass integral we obtain

$$\int_T b_{m,i} b_{n,j} d(x, y) = \int_0^1 \hat{b}_m^{(\eta)} \hat{b}_n^{(\eta)} d\eta \int_0^\infty \hat{b}_i^{(\xi)} \hat{b}_j^{(\xi)} h_\xi (h_\eta + (a+b)\xi) d\xi. \quad (27)$$

Due to the inverse Jacobian J^{-1} the stiffness integral is more complicated. We obtain

$$\begin{aligned} \int_T \nabla_{xy} b_{m,i} \cdot \nabla_{xy} b_{n,j} d(x, y) &= \\ &= \int_0^1 \partial_\eta \hat{b}_m^{(\eta)} (h_\xi^2 + (b - (a+b)\eta)^2) \partial_\eta \hat{b}_n^{(\eta)} d\eta \int_0^\infty \frac{\hat{b}_i^{(\xi)} \hat{b}_j^{(\xi)}}{h_\xi (h_\eta + (a+b)\xi)} d\xi \\ &+ \int_0^1 \partial_\eta \hat{b}_m^{(\eta)} \frac{b - (a+b)\eta}{h_\xi} \hat{b}_n^{(\eta)} d\eta \int_0^\infty \hat{b}_i^{(\xi)} \partial_\xi \hat{b}_j^{(\xi)} d\xi \\ &+ \int_0^1 \hat{b}_m^{(\eta)} \frac{b - (a+b)\eta}{h_\xi} \partial_\eta \hat{b}_n^{(\eta)} d\eta \int_0^\infty \partial_\xi \hat{b}_i^{(\xi)} \hat{b}_j^{(\xi)} d\xi \\ &+ \int_0^1 \hat{b}_m^{(\eta)} \hat{b}_n^{(\eta)} d\eta \int_0^\infty \partial_\xi \hat{b}_i^{(\xi)} \frac{h_\eta + (a+b)\xi}{h_\xi} \partial_\xi \hat{b}_j^{(\xi)} d\xi. \end{aligned} \quad (28)$$

For functions depending on η we use again the traces of finite element function in Ω_{int} . Hence, the bounded integrals over η can be treated in the usual way by quadrature formulas. For the infinite integrals we apply the identity (7) and the decomposition (6) to transform the ξ -direction into the Hardy space $H^+(D)$.

We have to take care of the factors ξ and $(\xi + c)^{-1}$ with a constant $c > 0$ in (27) and (28). For these we need one additional operator $\mathcal{D} : H^+(D) \rightarrow H^+(D)$ implicitly defined by

$$\mathcal{M}_{\kappa_0} \mathcal{L}\{(\bullet)f\} = \mathcal{M}_{\kappa_0} \{- (\mathcal{L}f)'\} = \mathcal{D} (\mathcal{M}_{\kappa_0} \mathcal{L}f).$$

Direct calculations yield

$$(\mathcal{D}F)(z) = \frac{(z-1)^2}{2i\kappa_0} F'(z) + \frac{z-1}{2i\kappa_0} F(z), \quad F \in H^+(D). \quad (29)$$

space domain	$\mathcal{M}_{\kappa_0} \mathcal{L}$	def.	implementation
f	$\frac{1}{i\kappa_0} \mathcal{T}_-(f_0, F)^\top$	(6)	(11)
f'	$\mathcal{T}_+(f_0, F)^\top$	(9)	(11)
$(\bullet)f$	$\mathcal{D}(\mathcal{M}_{\kappa_0} \mathcal{L}f)$	(29)	(30)
$\frac{1}{\bullet+c}f, c > 0$	$(\mathcal{D} + c \text{id})^{-1}(\mathcal{M}_{\kappa_0} \mathcal{L}f)$	(31)	num. inv. of $(\mathcal{D}_N + c \text{id})$

Table 1: Operators for the HSIE method; for the basic identity see (7)

If we use the set of trigonometric monomials up to the order N_ξ as basis functions in $H^+(D)$, we get the discrete operator

$$\mathcal{D}_{N_\xi} := \frac{1}{2i\kappa_0} \begin{pmatrix} -1 & 1 & & & & \\ 1 & -3 & 2 & & & \\ & 2 & -5 & 3 & & \\ & & \ddots & \ddots & \ddots & \\ & & & & N_\xi & -2N_\xi - 1 \end{pmatrix}. \quad (30)$$

Obviously it holds for the operator $(\mathcal{D} + c \text{id})^{-1}$

$$\mathcal{M}_{\kappa_0} \mathcal{L} \left\{ \frac{1}{\bullet+c} f \right\} = (\mathcal{D} + c \text{id})^{-1} (\mathcal{M}_{\kappa_0} \mathcal{L}f), \quad c > 0. \quad (31)$$

Note that both operators and the matrices \mathcal{D}_{N_ξ} and $(\mathcal{D}_{N_\xi} + c \text{id}_{(N_\xi+1) \times (N_\xi+1)})^{-1}$ are symmetric.

With the operators given in Table 1 and the identity (7) we are able to transform all integrals over ξ into the Hardy space $H^+(D)$. Using a Galerkin ansatz there with monomial basis functions, local matrices are obtained. For example the integral in (27) yields the local mass matrix

$$M := -\frac{2h_\xi}{i\kappa_0} T_{N_\xi,-}^\top (h_\eta \text{id}_{(N_\xi+1) \times (N_\xi+1)} + (a+b)\mathcal{D}_{N_\xi}) T_{N_\xi,-}. \quad (32)$$

In the same way we can treat the integrals in (28) and obtain the matrices

$$\begin{aligned} L_{00} &:= -\frac{2}{i\kappa_0 h_\xi} T_{N_\xi,-}^\top (h_\eta \text{id}_{(N_\xi+1) \times (N_\xi+1)} + (a+b)\mathcal{D}_{N_\xi})^{-1} T_{N_\xi,-}, \\ L_{01} &:= -2 T_{N_\xi,-}^\top T_{N_\xi,+}, \\ L_{10} &:= -2 T_{N_\xi,+}^\top T_{N_\xi,-}, \\ L_{11} &:= -\frac{2i\kappa_0}{h_\xi} T_{N_\xi,+}^\top (h_\eta \text{id}_{(N_\xi+1) \times (N_\xi+1)} + (a+b)\mathcal{D}_{N_\xi}) T_{N_\xi,+}. \end{aligned} \quad (33)$$

Remark 7. The method is applicable to a wide range of scalar Helmholtz-type problems. Since each segment in Ω_{ext} is treated separately, unbounded

inhomogeneities as e.g. waveguides are possible. Even coefficient functions n with unbounded support are possible, if there exist a segmentation of Ω_{ext} such that in each segment the function can be written in sums of terms $(\xi + a_j)^{k_j}$ (including negative powers) and functions depending on η

$$\hat{n}(\xi, \eta) = n \circ \mathbf{g}(\xi, \eta) = \sum (\xi + a_j)^{k_j} c_j(\eta), \quad a_j > 0 \text{ for } k_j < 0. \quad (34)$$

Remark 8. The exact statement of the tensor product space is due to the decomposition in (6) a little bit complicated. Another problem is, that the infinite integrals have to be bounded. This can be done by choosing test functions v , which decay fast enough and who are dense in the Hardy space after transformation. The details can be found in [11].

3. Perfectly Matched Layer

Exterior complex scaling was introduced by Simon [26] to facilitate the mathematical formulation of boundary conditions for the wave functions in quantum mechanics. It is shown by Chew and Weedon [3] that Bérenger's [2] PML developed for transient Maxwell's equations may be interpreted as a complex scaling of the exterior solution. Thus PML can be regarded as equivalent to exterior complex scaling.

Starting from a discretization of the exterior as in Fig. 8(b), the generalized radial coordinate is scaled by a constant complex factor σ , such that scattered outward radiating waves are damped exponentially. Using this discretization no special corner conditions are required. The exponential damping justifies to truncate the infinite domain some distance away from the boundary of the computational domain Ω_{int} and to impose homogeneous Dirichlet or Neumann boundary condition. This way the computational domain is surrounded by a finite layer. The convergence of the PML method for homogeneous exterior domains is analyzed by Lassas and Sommersalo [18] for the scattering problem and by Kim and Pasciak [17] for the resonance problem.

In our numerical experiments we compare the HSIE method with the adaptive PML method described in [27, 22]. The special feature of this PML is that the thickness of the layer is chosen adaptively based on an a posteriori estimate of the error introduced by truncating the layer and taking into account the discretization error of the interior. The distribution of the grid points is based on the observation that inside the PML short waves that require a fine grid to be resolved with a certain accuracy are damped much faster than long waves. Long waves in turn are well resolved on rather coarse grids.

4. Convergence test: A strip waveguide

In this section we compare different discretizations of the exterior domain for the Hardy space infinite element method applied to (17) with $\kappa = \frac{2\pi}{1.5}$, the

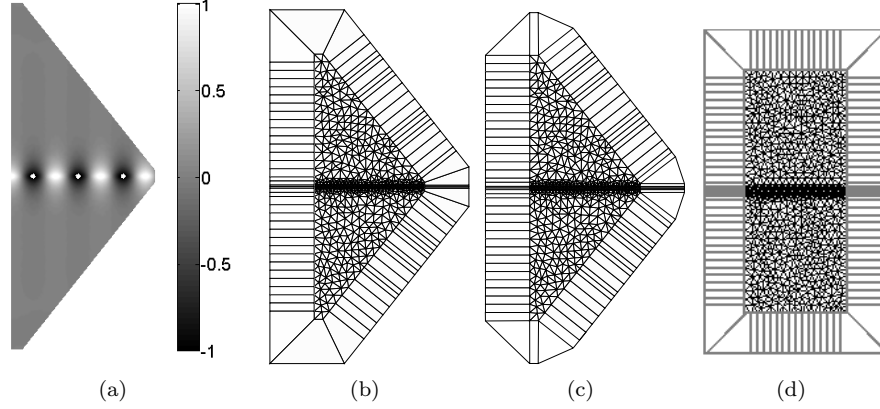


Figure 5: a) real part of u_i ; b,c) 1st mesh with two different exterior discretizations; d) 2nd mesh

refraction index

$$n(x, y) = n(y) = \begin{cases} n_2^2 & y \in (-a, a) \\ n_1^2 & y \in \mathbb{R} \setminus (-a, a) \end{cases} \quad (35)$$

and $a = 0.0365$, $n_1 = 1.45$ and $n_2 = 3.4$. The incoming wave is given by $u_i(x, y) = v(y)e^{i\kappa_x x}$, with

$$v(y) = \begin{cases} C_1 e^{\sqrt{\kappa_x^2 - n_1^2 \kappa^2} y} & , y \leq -a \\ C_2 e^{-i\sqrt{n_2^2 \kappa^2 - \kappa_x^2} y} + C_3 e^{i\sqrt{n_2^2 \kappa^2 - \kappa_x^2} y} & , y \in (-a, a) \\ C_4 e^{-\sqrt{\kappa_x^2 - n_1^2 \kappa^2} y} & , y \geq a \end{cases} \quad (36)$$

for $\kappa_x > 0$ and complex coefficients C_1, C_2, C_3 and C_4 , which have to ensure the continuity of v and v' in \mathbb{R} .

Remark 9. The incoming wave should satisfy the Helmholtz equation. Plugging the ansatz $u_i(x, y) = v(y)e^{i\kappa_x x}$ into (17) leads to the eigenvalue problem

$$(-\partial_y^2 - \kappa^2 n) v = -\kappa_x^2 v$$

for the eigenpair $(\kappa_x^2, v) \in \mathbb{R} \times H^2(\mathbb{R})$. If the jump in the refraction index n is large enough, such an $\kappa_x \in (n_1 \kappa, n_2 \kappa)$ exist and the corresponding eigenfunction v is exponentially decaying for $y \rightarrow \pm\infty$ and oscillating in $(-a, a)$.

We solved the problem for strip waveguide for the two different meshes in Fig. 5. The incoming wave is coupled via the jump conditions described in section 2.2 on the left vertical boundary part of the domain, which is chosen sufficiently large, so that u_i can be set to 0 in the lower and upper left corner. In order to test the Hardy space method the right vertical boundary is for one

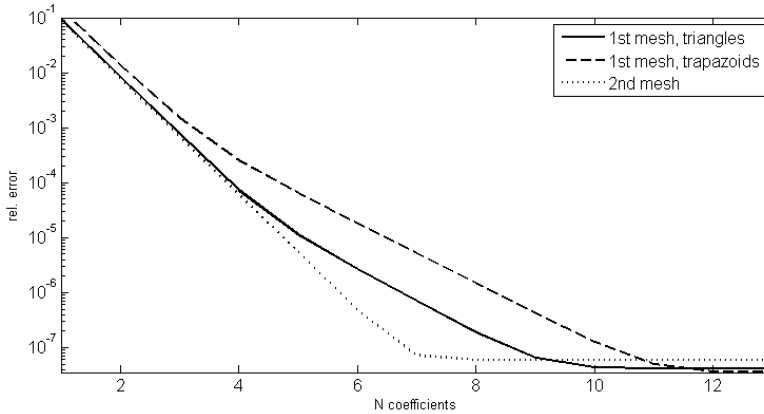


Figure 6: Relative $H^1(\Omega_{\text{int}})$ error of the Hardy space method vs. the number of degrees of freedom in radial direction

part of the computations very small. In the area around the right waveguide port the boundary (and with it the Hardy space method) has a big influence on the numerical solution, which should approximate the incoming field u_i .

For the exterior domain two different types of discretization are used: First we combined infinite strips with infinite triangles (Sec. 2.3.1). Second we used the trapezoids of section 2.3.2. As shown in Fig. 5 the rays are chosen in normal direction to the boundary and in corners as bisecting lines. For the computations we refined the diagrammed meshes once and used a high order method with polynomial order 7 for the finite element method in the interior domain.

Fig. 6 shows for the two different discretizations and the two meshes in Fig. 5 exponential convergence of the Hardy space method with respect to the number of degrees of freedom in radial direction. For the rectangular mesh both discretizations give the same result, since the influence of the upper and lower right corners on the discrete solution is very small. For the challenging mesh the trapezoidal discretization needs approximately one degree of freedom more than the non-uniform discretization. The computational costs for both discretizations are similar.

Fig. 7 shows the logarithm of the absolute value of the degrees of freedom in the Hardy space. The white domain in the middle is the interior domain and we have plotted only the degrees of freedom for the trapezoidal discretization. As expected from the one-dimensional case and from the theory about spherical exterior domains they decrease exponentially. Nevertheless, they do not decrease uniformly in all directions. Especially near to the exit port of the waveguide the decreasing factor is lower than in the other regions. For this reason a strategy to choose the number of Hardy modes adaptively is currently under investigation.

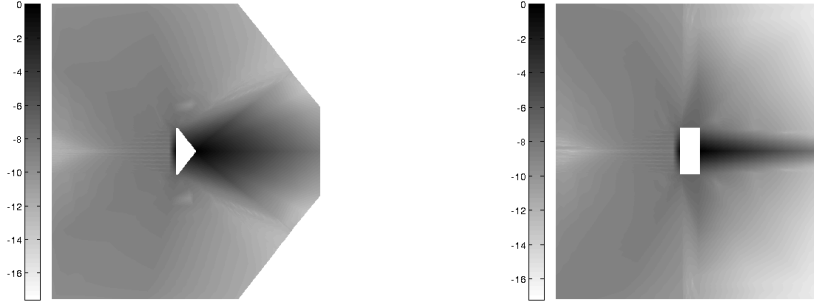


Figure 7: Logarithm of the absolute value of the degrees of freedom along the rays of the exterior domain for two different meshes in Fig. 5

5. Numerical example: a micro cavity resonator

This example is taken from Hammer [8] and consists of two waveguides coupled by a cavity. In order to exclude discretization effects originating from the resolution of the layout a geometry is chosen that is defined by polygons. The computational domain has a size of $3.5\mu\text{m} \times 4.546\mu\text{m}$, with a square cavity $a = b = 1.451\mu\text{m}$ in the center. We have $c = 0.2745\mu\text{m}$ and $d = 0.073\mu\text{m}$ in Fig. 8(a).

5.1. Scattering problem

To model the scattering of an incoming wave by an object the incoming waveguide mode of the last section is coupled by a jump condition of the Neumann and Dirichlet data at the left vertical boundary part for two different wavenumbers $k_1 = \frac{2\pi}{1.5\mu\text{m}}$ and $k_2 = \frac{2\pi}{1.5759\mu\text{m}}$. k_2 is close to a resonance, whereas for k_1 the cavity has only little effect, which can be seen in Fig. 9. For k_2 the wave propagates through the cavity into the lower waveguide.

For these computations we used for the interior finite elements of 5th order and refined the coarse grid 8(b) three times uniformly. In the exterior domain we used the trapezoidal Hardy space infinite element method with the parameter $\kappa_0 = 8 + 5i$ and 30 degrees of freedom in order to discretize the Hardy space. In total we got approximately 200.000 degrees of freedom.

5.2. Resonance problem

Starting from a coarse mesh the interior is adaptively refined using a residual based error estimator [27]. On each refinement level the eigenvalue of the resonance problem is calculated. To evaluate the relative error in the eigenvalue, a reference resonance frequency if $\omega = 1.1951173e + 15 - 1.489202e + 13i$ is calculated on a very fine mesh using the PML. The wavelength of the resonance is $\lambda = 2\pi c/\omega$, where $c = 299792458\text{m/s}$ is the speed of light. Hence the wavenumber $k_1 = 2\pi/\lambda_1 = \frac{2\pi}{1.5759\mu\text{m}}$ of Section 5.1 is close to the resonance.

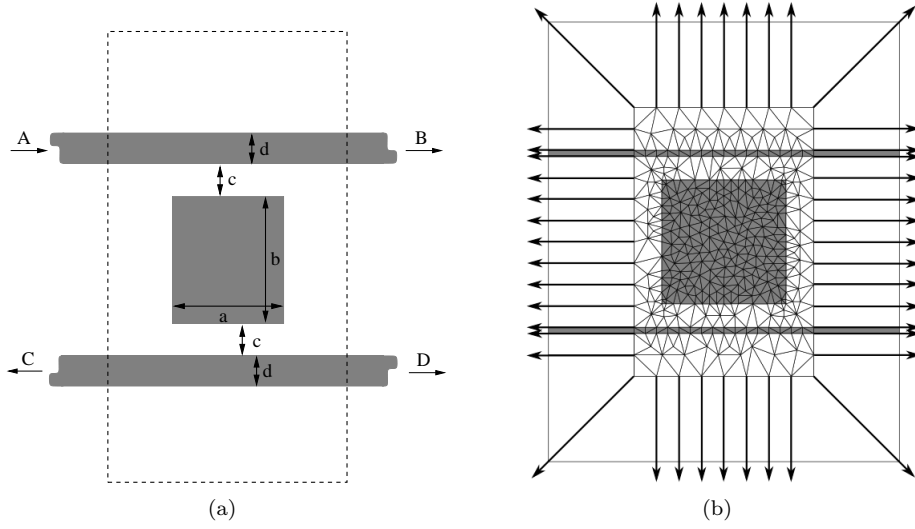


Figure 8: a) Schematic geometry of the micro cavity resonator. b) Coarse grid discretization by triangles in the interior and trapezoids in the exterior. ($a = b = 1.451\mu\text{m}$, $c = 0.2745\mu\text{m}$ and $d = 0.073\mu\text{m}$)

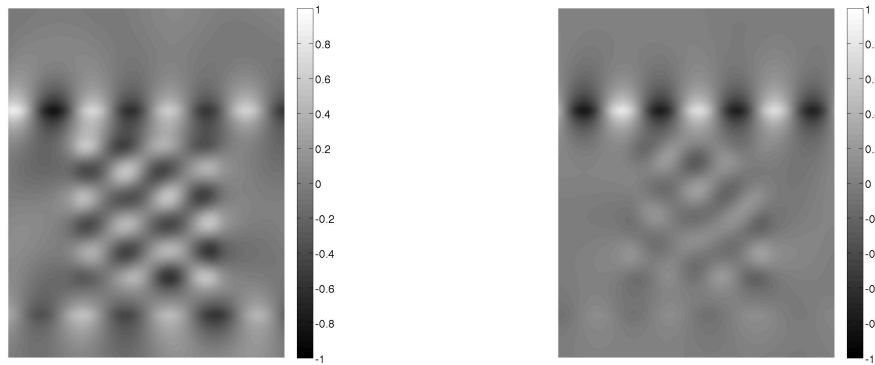


Figure 9: Real part of a the solution to the scattering problem with wavelength $k = \frac{2\pi}{1.5759\mu\text{m}}$ (left) and $k = \frac{2\pi}{1.5\mu\text{m}}$ (right)

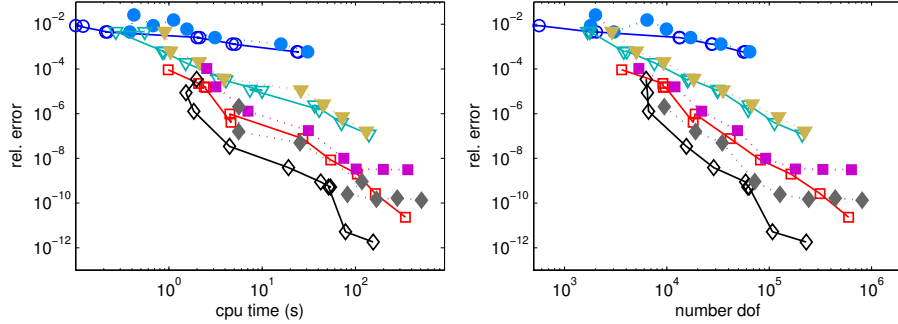


Figure 10: Comparison: PML (dashed line with filled markers) with HSIE (solid line) with $\kappa_0 = 5 + 3i$ for various finite element degrees: 1 (\circ), 2 (\triangle), 3 (\square), and 4 (\diamond). Left: Work-precision diagram showing the relative error in the eigenvalue vs. cpu-time in seconds. Right: Convergence of PML and HSIE showing the relative error in the eigenvalue vs. number of degrees of freedom.

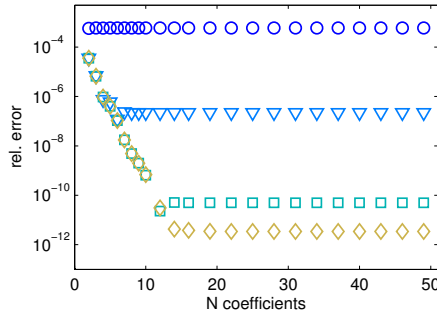


Figure 11: Rel. error in the eigenvalue vs. number of Hardy-modes ($\kappa_0 = 5 + 3i$) for finite elements of degree $p = 1$ (\circ), $p = 2$ (\triangle), $p = 3$ (\square), and $p = 4$ (\diamond).

In this example two methods, PML and HSIE, to realize transparent boundary conditions are compared. The results for the PML are obtained using the adaptive PML as described in Section 3. The results for the HSIE are obtained using $N = 2, \dots, 50$ Hardy modes and selecting the best result. 10 shows the error versus the cpu time (left) and the total number of degrees of freedom (right) that is required to solve the eigenvalue problem on the finest refinement level. The initial guess is $1.195 \cdot 10^{15} - 0.01489 \cdot 10^{15}i$. The HSIE method in this example yields results that are better or at least as good the results obtained with the PML method. The implementation was done in the C++ code JCMSuite [15].

Fig 11 shows the super algebraic convergence in the number of Hardy modes. For these calculations $\kappa_0 = 5 + 3i$. The number of degrees of freedom to discretize the interior is about 944000 for $p = 1$, 169000 for $p = 2$, 121000 for $p = 3$ and 103000 for $p = 4$. For low accuracies very few Hardy modes are required, e.g. to reduce the approximation error of the transparent boundary condition

below 10^{-6} 7 Hardy modes are sufficient. To obtain a relative error of about 10^{-10} almost one third of the total number of degrees of freedom is spent on approximating the transparent boundary condition.

6. Conclusions

We have presented here the Hardy space infinite element method from a practical point of view. In this form inhomogeneous exterior domains can be treated as well as arbitrary convex polygons as artificial boundaries. The numerical results show superalgebraic convergence with respect to the degrees of freedom in the Hardy space, i.e. the degrees of freedom in the radial direction. The method preserves the eigenvalue structure and is therefore well suited for solving resonance problems. Compared to former realizations of the pole condition like the *cut function approach* ([25]) it is not possible to recover the solution in the exterior domain directly. In this point the HSIE method behaves like perfectly matched layer methods: The degrees of freedom in the exterior domain are physically irrelevant. They just provide for a good approximation at the exact transparent boundary condition on the artificial boundary.

A comparison of the results of the HSIE and the used PML is already given in the last section. From the point of implementation the HSIE requires a new (*in*)finite element, whereas the PML only changes the variational formulation of the problem. On the other hand the HSIEs show exponentially convergence, while the PML inherits the convergence order of the used finite element method. One basic difference between both methods is given by the nature of the discretizations. For the PML there exist two steps: First truncating the infinite PML-domain and than discretizing the finite layer using finite elements. The HSIE uses a (transformed) variational formulation of the whole infinite domain. The only discretization results from the Galerkin method.

The HSIE is not restricted to scalar, time-harmonic problems. In [21] a similar version of the method is used for solving time-dependent problems. Moreover, there exist first results for Maxwell's equations.

Acknowledgment

The fruitful and stimulating discussions with T. Hohage, F. Schmidt and L. Zschiedrich are sincerely acknowledged.

References

- [1] R. J. Astley. Infinite elements for wave problems: A review of current formulations and an assessment of accuracy. *Internat. J. Numer. Methods Engrg.*, 49(7):951–976, 2000.
- [2] J.-P. Berenger. A perfectly matched layer for the absorption of electromagnetic waves. *J. Comput. Phys.*, 114(2):185–200, 1994.

- [3] W. C. Chew and W. H. Weedon. A 3d perfectly matched medium from modified Maxwell's equations with stretched coordinates. *Microwave Optical Tech. Letters*, 7:590–604, 1994.
- [4] L. Demkowicz and K. Gerdes. Convergence of the infinite element methods for the Helmholtz equation in separable domains. *Numer. Math.*, 79:11–42, 1998.
- [5] P. L. Duren. *Theory of H^p spaces*. Pure and Applied Mathematics, Vol. 38. Academic Press, New York, 1970.
- [6] D. Givoli. High-order local non-reflecting boundary conditions: a review. *Wave Motion*, 39:319–326, 2004.
- [7] M. J. Grote and J. B. Keller. Nonreflecting boundary conditions for Maxwell's equation. *J. Comput. Phys.*, 139:327–324, 1998.
- [8] M. Hammer. Resonant coupling of dielectric optical waveguides via rectangular microcavities: the coupled guided mode perspective. *Optics Communications*, 214(1-6):155–170, 2002.
- [9] S. Hein, T. Hohage, W. Koch, and J. Schöberl. Acoustic resonances in high lift configuration. *J. Fluid Mech.*, 582:179–202, 2007.
- [10] K. Hoffman. *Banach spaces of analytic functions*. Prentice-Hall Series in Modern Analysis. Prentice-Hall Inc., Englewood Cliffs, N. J., 1962.
- [11] T. Hohage and L. Nannen. Hardy space infinite elements for scattering and resonance problems. *SIAM J. Num. Analysis*, 47(2):972–996, 2009.
- [12] T. Hohage, F. Schmidt, and L. Zschiedrich. A new method for the solution of scattering problems. In B. Michielsen and F. Decavèle, editors, *Proceedings of the JEE'02 Symposium*, pages 251–256, Toulouse, 2002. ONERA.
- [13] T. Hohage, F. Schmidt, and L. Zschiedrich. Solving time-harmonic scattering problems based on the pole condition. I. Theory. *SIAM J. Math. Anal.*, 35(1):183–210 (electronic), 2003.
- [14] G. C. Hsiao and W. L. Wendland. *Boundary integral equations*, volume 164 of *Applied Mathematical Sciences*. Springer-Verlag, Berlin, 2008.
- [15] JCMwave GmbH. www.jcmwave.com.
- [16] B. Kettner. Ein Algorithmus zur prismatoidalen Diskretisierung von unbeschränkten Außenräumen in 2D und 3D. Master's thesis, Freie Universität Berlin, 2007.
- [17] S. Kim and J. E. Pasciak. The computation of resonances in open systems using a perfectly matched layer. *Math. Comp.*, 2008.

- [18] M. Lassas and E. Somersalo. On the existence and the convergence of the solution of the pml equations. *Computing*, 60:229–241, 1998.
- [19] M. Lenoir, M. Vullierme-Ledard, and C. Hazard. Variational formulations for the determination of resonant states in scattering problems. *SIAM J. Math. Anal.*, 23:579–608, 1992.
- [20] L. Nannen. *Hardy-Raum Methoden zur numerischen Lösung von Streu- und Resonanzproblemen auf unbeschränkten Gebieten*. PhD thesis, University of Göttingen, Der Andere Verlag, Tönning, 2008.
- [21] D. Ruprecht, A. Schädle, F. Schmidt, and L. Zschiedrich. Transparent boundary conditions for time-dependent problems. *SIAM J. Sci. Comput.*, 30(5):2358–2385, 2008.
- [22] A. Schädle, L. Zschiedrich, S. Burger, R. Klose, and F. Schmidt. Domain decomposition method for Maxwell’s equations: Scattering off periodic structures. *J. Comput. Phys.*, 226:477–493, 2007.
- [23] F. Schmidt. An alternative derivation of the exact dtn-map on a circle. Technical Report SC 98-32, Konrad-Zuse-Zentrum Berlin, 1998.
- [24] F. Schmidt. A new approach to coupled interior-exterior Helmholtz-type problems: Theory and algorithms. Habilitation, Freie Universität Berlin, 2002.
- [25] F. Schmidt, T. Hohage, R. Klose, A. Schädle, and L. Zschiedrich. Pole condition: A numerical method for Helmholtz-type scattering problems with inhomogeneous exterior domain. *J. Comput. Appl. Math.*, 218(1):61–69, 2008.
- [26] B. Simon. The definition of molecular resonance curves by the method of exterior complex scaling. *Phys. Lett. A*, 71A(2, 3), 1979.
- [27] L. Zschiedrich, S. Burger, R. Klose, A. Schädle, and F. Schmidt. JCMmode: An adaptive finite element solver for the computation of leaky modes. In Y. Sidorin and C. A. Wächter, editors, *Integrated Optics IX*, volume 5728 of *Proc. SPIE*, pages 192–202, 2005.
- [28] L. Zschiedrich, R. Klose, A. Schädle, and F. Schmidt. A new finite element realization of the perfectly matched layer method for Helmholtz scattering problems on polygonal domains in two dimensions. *J. Comput. Appl. Math.*, 188(1):12–32, 2006.